05

Mechanisms of magnetoelectric effects in oxide multiferroics with a perovskite praphase

© Z.V. Gareeva[1,2], A.K. Zvezdin[3,4], N.V. Shulga[1], T.T. Gareev[2], X.M. Chen[5]

[1] Institute of Molecule and Crystal Physics, Subdivision
of the Ufa Federal Research Centre of the Russian Academy of Sciences,
Ufa, Russia
[2] Bashkir State University,
Ufa, Russia
[3] Prokhorov General Physics Institute of the Russian Academy of Sciences,
Moscow, Russia
[4] Lebedev Physical Institute, Russian Academy of Sciences,
Moscow, Russia
[5] Laboratory of Dielectric Materials, Zhejiang University,
Hangzhou, People's Republic of China, 310027

E-mail: gzv@anrb.ru

Magnetoelectric effects are discussed in multiferroics with the perovskite structure: bismuth ferrite, rare-earth orthochromites, and Ruddlesden–Popper structures belonging to the trigonal, orthorhombic, and tetragonal syngonies. The influence of structural distortions on magnetic and ferroelectric properties is studied, possible magnetoelectric effects (linear, quadratic, inhomogeneous) in these materials are determined, and expressions for the linear magnetoelectric effect tensor are given. Macroscopic manifestations of the inhomogeneous magnetoelectric effect in multiferroic nanoelements are considered.

Keywords: multiferroics, magnetoelectric effect, perovskites, symmetry.

1. Introduction

The development of information technology and spintronics stimulates the search and development of new materials with effective functional properties. In this respect, multiferroic structures are promising, in which several types of orders are implemented. Magnetoelectric components based on multiferroics are planned to be used as buffer elements of logic devices, the principle of operation of which is based on magnetoelectric and spin-orbital communication (MESO), magnetic memory of arbitrary access (MRAM)as well as elements of neural network technologies [1–4]. In this connection, the need to search for optimal conditions for the implementation of magnetoelectric effects and the integration of multiferroics qualities with topological properties of materials arises.

Magnetoelectric materials include a large group of single-phase multiferroics — compounds with ABO_3 — perovskite praphase, among which the best known multiferroics are bismuth ferrite ($BiFeO_3$), rare earth orthoferrites ($RFeO_3$) and orthochromites ($RCrO_3$) [5] also, topological insulators $Bi_xMn_{1-x}Te_2$, in which the magneto-electric effect (MEE) [6] has been recently discovered, can be considered as contenders for perovskite multiferroics; layered structures of the Ruddlesden–Popper (RP) [7–10] type are attracting increasing interest due to the discovery of high-temperature ferroelectric properties [10] in them. There are significant differences in the manifestation of FE properties in the materials listed, which is due to the different degree of distortion of the structure of the perovskite and the difference in the symmetry groups corresponding to the specific crystal structure. The degree of distortion of the crystalline structure affects the magnetic and ferroelectric properties of the multiferroics. In this regard, identifying the mechanisms responsible for the interaction of the crystallographic, ferroelectric and magnetic subsystems of the ABO_3 type is an important task, which is necessary for the successful implementation of instruments and devices, MEE-based.

The purpose of this study is to highlight the main mechanisms of MEE in ABO_3 — multiferroics of various symmetries, focusing on crystallographic distortions; consider the implementation conditions of linear, quadratic and inhomogeneous MEE, analyze spin-orbital effects, micromagnetic structures and polar states in multiferroic films of limited size.

2. Magnetoelectric effects in multiferroics of perovskite structure

In this section, using group-theoretic analysis methods, we analyze the crystal structure, the ferroelectric and

magnetic properties of materials with perovskite structure ($BiFeO_3$, $RCrO_3$, $Ca_{3-x}R_xFe_2O_7$).

2.1. Bismuth ferrite $BiFeO_3$ is one of the most famous high-temperature multiferroics, the temperature of ferro-electric and magnetic ordering in it are $T_C = 1083$ K, $T_N = 643$ K [11,12]. $BiFeO_3$ crystallizes in the symmetry group $R3c$, the main crystallographic distortions of ABO_3 perovskite are as follows: (i) displacement of Bi and Fe ions along the $\langle 111 \rangle$ axis, (ii) deformations of oxygen octahedrons of FeO_6 and (iii) anti-rotation of oxygen octahedrons around the $\langle 111 \rangle$ axis. It is the presence of these types of distortions that accounts for $BiFeO_3$'s ferroelectric and magnetic properties. Thus, according to the estimates made in work [13], the value of spontaneous ferroelectric polarization is related to distortions of the form (i), (ii) and can be calculated by the formula

$$P_x = \frac{4e}{V}(3\xi_{Bi} - 4\xi_{O1} - 2\xi_{O3}), \qquad (1)$$

where e — elementary charge, V — volume of the unit cell, ξ_{Bi} — displacement of Bi ions corresponding to (i) distortion, ξ_{O1} and ξ_{O3} — displacement of oxygen ions corresponding to (ii) — distortion. Note that this simple estimate is well supported by experimental measurements [14,15]. In magnetic relation, $BiFeO_3$ is a weak ferromagnet with antiferromagnetic ordering of the G-type, whereby the occurrence of the resulting magnetization is associated with the rotation of oxygen octahedrons [16], its magnitude can be calculated by formula [17]:

$$\mathbf{M} = \frac{V_0 a^2}{6J}\mathbf{\Omega} \times \mathbf{L} + \frac{V_0 a^2}{6J}\sum_{n=1}^{6}(\mathbf{n}_n \times \xi_{O_n}), \qquad (2)$$

where V_0 — constant, a — lattice parameter, J — exchange constant, $\mathbf{n}_n$ — unit vector oriented along one of the crystallographic axes $\langle 100 \rangle$.

$BiFeO_3$'s symmetry allows the existence of linear magnetoelectric effect (MEE), in particular linear electric polarization dependence on magnetic field, as well as the existence of spatially-modulated structures, stabilized b they Dzyaloshinskii–Moriya interaction (DMI). The dependence of electric polarization on the magnetic field is expressed through the MEE tensor α_{ij} [12], the magnitude of which in monocrystals and bismuth ferrite films is still the subject of active scientific discussions. This is due not only to a fundamental physical interest in the subject, but also to the prospects of practical use of $BiFeO_3$ crystals and films with high values of α_{ij}. In this regard, we will focus on some recent research results, focusing on the correlation of the ferroelectric and magnetic properties of $BiFeO_3$ with structural distortions of perovskite, which is also to be expected in the magnetoelectric coupling factor α_{ij}.

The linear MEE mechanism in $BiFeO_3$ has been theoretically investigated, in particular in work [18], where it has been shown that the value of the linear MEE tensor is dependent on structural distortion, including the sensitivity of the distortion parameter of order Ω_0 to an external electric field ($\mathbf{E}$), which is determined by dielectric susceptibility tensor

$$\hat{\eta} = \begin{pmatrix} \eta_\perp & 0 & 0 \\ 0 & \eta_\perp & 0 \\ 0 & 0 & \eta_\parallel \end{pmatrix}, \qquad (3)$$

where $\eta_\perp$ and $\eta_\parallel$ — tensor components $\hat{\eta}$, determine dielectric receptivity parameter Ω_0 to electric field oriented perpendicular and along the direction of spontaneous electric polarization $\mathbf{P}_s \parallel \langle 111 \rangle$. In this case, the linear MEE tensor expressed through the tensor components of the $\hat{\eta}$, has the appearance of

$$\alpha_{ij}^{BiFeO_3} = 4\pi\chi_\perp \frac{H_D^0}{\Omega_0}\begin{vmatrix} 0 & \eta_\perp L_z & -\eta_\perp L_y \\ -\eta_\perp L_z & 0 & \eta_\perp L_x \\ \eta_\parallel L_y & \eta_\parallel L_x & 0 \end{vmatrix}, \qquad (4)$$

where $\chi_\perp$ — transverse magnetic susceptibility ($\chi_\perp \sim 5 \cdot 10^{-5}$), H_D^0 — value of the Dzyaloshinskii field ($H_D^0 \approx 1.4 \cdot 10^5$ Oe), Ω_0 — the axial vector of the distortion order parameter, the direction coincides with the axis direction $\langle 111 \rangle$, and its magnitude is 11^0–14^0; L_i, $i = x, y, z$ — components of the antiferromagnetic vector. Considering that $|\mathbf{L}| = 1$, we give an estimate of the MEE tensor components [18] $\alpha_\perp \sim 0.67$ V/(cm·Oe), $\alpha_\parallel \sim 9.81$ V/(cm·Oe), which is consistent with the results of experimental studies of the MEE properties of BiFeO-based heterostructures $BiFeO_3$ [19]. Note that such a result is possible in film structures of $BiFeO_3$, in which the strict deformation leads to the suppression of the space-modulated structure of cycloidal type [20], which is the main magnetic state of $BiFeO_3$, whereas in $BiFeO_3$ monocrystals the linear MEE cannot be realized due to the presence of a spin cycloid, since in this case the average value of $\langle \mathbf{L} \rangle = 0$, which leads to zeroing of the components of α_{ij} tensor, as seen from formula (4). The alternative to $BiFeO_3$–containing heterostructures is $BiFeO_3$-ceramic, which also manages to implement linear MEE by substituting rare earth ions for Bi ions. Researches in this direction are conducted, since 1990, up to the present day, the received results specify the possibility of realization of MEE in compositions of $Bi_{1-x}R_xFeO_3$ with rare-earth ions ($R = Gd, Dy, La, Lu$) [20–27]. Below we will focus on the results of a paper in which the appearance of MEE in R-doped single crystals $BiFeO_3$ is explained by reduced symmetry. In works [13,20–25] it has been shown that a series of structural phase transitions, accompanied by a decrease in symmetry, is observed when the concentration of rare-earth x ions changes, from trigonal $R3c$ (C_{3v}^6) to rhombic $Pn2a_1$ (C_{2v}^9) (C_{3v}^6–C_1^1–D_2^6–D_2^5–C_{2v}^9) [13,25], and as was shown in [28], to $Pbnm$ ($R3c$–$Pna2_1$–$Pbnm$). Experimental studies performed in [28] indicate the appearance of magnetization and an increase in magnetoelectric coefficient value α in $Bi_{0.82-x}La_xLu_{0.18}FeO_3$ ceramics to 2 mV/(cm·Oe), however, we note that the physical mechanisms responsible

for the appearance of the magnetoelectric properties in these structures are not fully elucidated.

As shown in [29–31], in the presence of magnetically active f-ions (Gd, Dy, Tb) in structures with *Pbnm* symmetry, MEE can arise due to antiferromagnetic (center-asymmetric) ordering of rare-earth ions, which is determined by the antiferromagnetic vector **l** of the rare earth ions, whose components are classified by irreducible representations of the symmetry group *Pbnm* (D_{2h}) [33,34]. In the case of replacement of Bi ions by La ions, as shown in [25], the magnetoelectric properties of $Bi_{1-x}La_xFeO_3$ may be due to a quadratic MEE, which partially helps to explain the smaller value of the MEE coefficient obtained in [28] compared to the experimental values α_{ME} [19].

2.2. Rare earth orthochromites and orthoferrites ($RCrO_3$ and $RFeO_3$) are low-temperature multiferroics ($T_C \sim 130-250$ K) with weakly pronounced magnetoelectric properties, nevertheless the possibility of the realization of MEE in these materials is of great scientific interest. $RCrO_3$ and $RFeO_3$ crystallize in non-polar symmetry group *Pbnm*, the mechanisms of the appearance of MEE are actively discussed in the literature. In accordance with the results of experimental studies [35–37], also see the citations in [38], in rare-earth orthoferrites and orthochromites there is MEE realized under certain conditions. Thus, work [30] gives data on the linear MEE ($\alpha_{zz} \sim 2.4 \cdot 10^{-2}$ esu) that was experimentally observed in $DyFeO_3$ at temperatures below the antiferromagnetic ordering temperature of Dy^{3+} ($T_N \sim 4$ K) ions. In this case, as mentioned above, one of the physical mechanisms responsible for the magnetoelectric effect is the antiferromagnetic ordering of rare-earth ions (Dy^{3+}), which are classified according to the same irreducible representations as the electric polarization vector components; this mechanism was theoretically investigated in [29]. Experimental studies [35–37] indicate the appearance of ferroelectric properties of orthochromites ($YCrO_3$, $RCrO_3$ with various rare earth ions) after polishing crystals in the electric field, which leads to the appearance of electric polarization, the process is accompanied by spin-reorientation phase transitions, which points to the magneto-electric nature of the effect. Below we discuss a general approach to the analysis of the magnetoelectric properties of orthochromite and orthoferrite single crystals based on the consideration of crystallographic distortions and the symmetry analysis of the structural, magnetic, and ferroelectric order parameters. The main crystallographic distortions of ABO_3 perovskite leading to structures of the form $RCrO_3$ ($RFeO_3$) include the rotation of CrO_6 (FeO_6) oxygen octahedrons around crystallographic direction [110], as well as the displacements of the R^{3+} and O^{2-} ions (ξ_q, $q = R, O$) relative to their centrosymmetric positions in the ABO_3 perovskite structure. As was shown in [38], a dipole moment is induced in the vicinity of Cr^{3+} ions, which results from displacements of oxygen ions (ξ_q). In the frame of the dot charge model, the value of dipole

moment $\mathbf{d}_q = q\mathbf{r}_q$ is determined by the radius vector

$$\mathbf{r}_q = \frac{\left(+\frac{3}{8}e\right)\sum\limits_{i=1}^{8}\xi_{R_i} + \left(-\frac{2}{2}e\right)\sum\limits_{i=1}^{6}\xi_{O_i}}{\left|8\cdot\left(+\frac{3}{8}e\right) + 6\cdot\left(-\frac{2}{2}e\right)\right|},$$

expressed through distortion (ξ_q, where $q = R^{3+}, O^{2-}$). In the absence of external influences, the dipole moments form an antiferroelectric structure, so in crystals with a symmetry group of *Pbnm* no electrical polarization occurs and as a result, ferroelectric and magnetoelectric effects are absent.

In $RCrO_3$ ($RFeO_3$, 3 types of magnetic exchange-bonded structures $\Gamma_1(A_x, G_y, C_z)$, $\Gamma_2(F_x, G_z, C_y)$, $\Gamma_3(F_z, A_y, G_x)$ are implemented, with weak ferromagnetism on the background of antiferromagnetic ordering of *G*-type. The components of the ferromagnetic vector **M** depend on the axial distortion parameter of order Ω_b. In orthophorrites and orthochromites, the vector Ω_b is oriented along the b — axis of the crystal ($\langle 010 \rangle$), its value is determined by the angle of rotation of oxygen octahedra.

$$\mathbf{M} = \left(\alpha_{xxz}\Omega_{bx}G_z, \alpha_{yyx}\Omega_{by}G_x, \alpha_{zyz}\Omega_{by}G_z\right). \quad (5)$$

As a result of $RFeO_3$ heat treatment or $RCrO_3$ electropolishing by an electric field, there is a decrease in symmetry to *Pnma*, in this case, the antiferroelectric structure of dipole moments is broken, which leads to the emergence of spontaneous electrical polarization and the emergence of MEE, which has been experimentally observed in work [35–37]. The MEE tensor can be calculated [31], using the table of irreducible representations of the *Pnma* group

$$\alpha_{ij}^{RCtO_3} = \begin{vmatrix} a_1 G_x(g_z G_y - g_y G_z) & a_2 g_z & a_3 g_x \\ a_2 g_z & a_1 G_x(g_z G_y - g_y G_z) & a_4 g_y \\ a_4 g_y & a_3 g_x & a_2 g_z \end{vmatrix},$$
$$(6)$$

where G_i, g_i — the antiferromagnetic vector components of the Cr^{3+}-sublattice and R^{3+}-sublattice, respectively.

2.3. Ruddlesden–Popper structures are layered structures derived from perovskites with the general chemical formula $A_{n+1}B_nC_{3n+1}$, in which A^{2+} and B-positions contain A^{2+} and B^{4+} — valence cations, and in C — C^{2-} anions, mainly oxygen anions (O^{2-}), where n — number of octahedral perovskite layers. Situations with $n = 1$ and $n = \infty$ are the extreme cases of RP. At $n = 1$, a 2D structure of the form A_2BO_4 consisting of perovskite cells ABO_3 separated by AO layers is realized; at $n = \infty$ RP is an infinite series of perovskite cells. In recent years, the Ruddlesden–Popper (RP) structures have attracted considerable attention due to the discovery in them of ferroelectric properties that can be implemented at room temperatures, and the prospects of high-temperature MEE [10,39]. When temperature changes in RP structures, there are phase transitions from the tetragonal $I4/mmm$ phase to orthorhombic through a series of intermediate phases. In the temperature range $T < T_N < T_{RT}$ ($T_N \sim 134$ K) antiferromagnetic (AFM) ordering of G- or C-type is realized in the $Ca_3Mn_2O_7$

compounds, in work [8] it was shown that exchange-bonded structures of the form $(G_xF_yG_z)$, $(F_xG_yA_z)$, $(A_xC_yF_z)$ can be formed in them. It can be shown that in these structures symmetry allows linear MEE, and the tensor α_{ij}^{R-P} has the form of

$$\alpha_{ij}^{R-P} = \begin{vmatrix} \gamma_3 G_z & 0 & \gamma_2 G_x \\ 0 & \gamma_3 G_z & \gamma_2 G_y \\ \gamma_4 G_x & \gamma_4 G_y & \gamma_5 G_z \end{vmatrix}. \tag{7}$$

Note that experimental studies of $[1-x](Ca_ySr_{1-y})_{1.15}Tb_{1.85}Fe_2O_7$ [39] structures have confirmed the presence of linear MEE in these materials at certain concentrations of $0.0 \le x \le 0.30$, $y = 0.563$.

3. Inhomogeneous magnetoelectric effects in multiferroic nano-elements

In this section we will briefly discuss inhomogeneous magnetoelectric effects that can be realized in multiferroic systems of restricted geometry. To do this, we consider a nano-element, which is a film of multiferroic, the symmetry of which allows the existence of a inhomoheneous magnetoelectric effect, and due to spin-orbital bond with the orienting substrate in the system, the interaction of the Dzyaloshinskii–Moriya interaction occurs. The energy of such a system is

$$F = \iint d^2r \left(A(\partial_\mu m_\alpha)^2 + F_{me} + F_{DMI} - Km_z^2 \right.$$
$$\left. - \frac{1}{2} M_s \mathbf{m} \cdot \mathbf{H}_m - M_s \mathbf{m} \cdot \mathbf{H} \right), \tag{8}$$

where A — exchange interaction constant, K — magnetic anisotropy constant, $\alpha, \mu = x, y, z$, $\mathbf{m} = \mathbf{M}/M_s$ — unit magnetization vector, $\mathbf{H}_m$ — magnetostatic field, $\mathbf{H}$ — external magnetic field (we will consider the situation when the field $\mathbf{H}$ is oriented along the normal to the film surface). $F_{me} = \gamma \mathbf{P}[\mathbf{M}(\nabla\mathbf{M}) - (\mathbf{M}\nabla)\mathbf{M}]$ — magnetoelectric energy, γ — parameter of non-uniform magnetoelectric interaction, F_{DMI} — Dzyaloshinskii–Moriya energy. In the case under consideration F_{DMI} has the form

$$F_{DM} = t \iint D \left[\left(m_x \frac{\partial m_z}{\partial x} - m_z \frac{\partial m_x}{\partial x} \right) \right.$$
$$\left. + \left(m_y \frac{\partial m_z}{\partial y} - m_z \frac{\partial m_y}{\partial y} \right) \right] d^2r, \tag{9}$$

where the t — thickness of the nano-element. Electrical polarization is calculated by formula

$$\mathbf{P} = \gamma \chi_e \left[(\mathbf{M}\nabla)\mathbf{M} - \mathbf{M}(\nabla\mathbf{M}) \right]. \tag{10}$$

The Dzyaloshinskii–Moriya interaction at the interface (DMI) can lead to the stabilization of inhomoheneous magnetic structures of different topology. The type of magnetic structure depends on a combination of geometric factors (nano-element size), internal parameters of the

system (A, K, M_s, D) and external influences. When parameters change, there are transitions between magnetic states. Electrical polarization is realized in the vicinity of the inhomoheneous magnetization distribution in accordance with the concept of non-homogeneous MEE.

As an example, consider a nano-element with dimensions $a \times a \times t$ nm^3 and material parameters: $A = 2.9 \cdot 10^{-12}$ J/m, $K = 1 \cdot 10^3$ J/m^3, $-0.5 < D < 0.5$ mJ/m^2. Possible types of micromagnetic configurations arising due to the action of the magnetic field $\mathbf{H} = (0, 0, H)$, calculate using the package OOMMF [40], the size of the lattice $5 \times 5 \times 3$ nm^3. Figure (a) shows examples of four topological micromagnetic structures, which are realized in a nano-element with a size of $a = 50$ nm, $t = 30$ nm at $D = 0.6$ mJ/m^2 during re-magnetization process. Note that the initial state in $|H| > 16$ kOe field is a homogeneous state in which the magnetization vector $\mathbf{M} = (0, 0, M_s)$ is uniformly distributed across the nano-element volume.

Consider first the demagnetization process, during which phase transitions are observed between the micromagnetic states of different topology (see figure, part a). Here is a brief description of these conditions and the conditions under which they are observed. The range of $0 < H < 16$ kOe fields implements state 1: (V+) — vortex positive polarity, magnetization vector in the center of the vortex V+ is oriented towards the direction of the magnetic field. In the range of $-10 < H < 0$ kOe fields in the nano-element state 2 is realized: (DW+) — system of two vortices V-, separated by 180° domain boundary, oriented on the left-diagonal nano-element. Further demagnetization leads to state 4: (V-) — a vortex with opposite polarity, which exists in the range of $H < -10$ kOe, at saturation we get a uniform magnetized state of $\mathbf{M} = (0, 0, -M_s)$.

The situation is similar when the nano-element is magnetized. When increasing the magnetic field size, the following transitions occur: a homogeneous state of $\mathbf{M} = (0, 0, -M_s)$ — state 4: vortex V- with negative polarity $(-16 < H < 0$ kOe), further state 3: (DW-) 180° domain boundary oriented by right diagonal nano-element $(0 < H < 10)$, then state 1: vortex V+ $(H > 10$ kOe) and transition to homogeneous state $\mathbf{M} = (0, 0, M_s)$. Due to the heterogeneous magnetoelectric effect in the vicinity of the heterogeneous magnetization distribution in states 1, 2, 3, 4, there is an electrical polarization of $\mathbf{P}(\mathbf{r}_i)$. As a result, in the nano-element, along with the micromagnetic structures, forms polar ferroelectric structures in which the distribution of the vector $\mathbf{P}(\mathbf{r}_i)$ is determined by the magnetic state. The magnitude of polarization, the number and properties of polar structures are determined by the topology of the magnetic texture, which in turn depends on the internal parameters of the system (magnetic anisotropy, Dzyaloshinskii–Moriya constant), geometrical factors (the shape of the sample, transverse and longitudinal dimensions), as well as external influences (magnetic or electric field). The change in the external magnetic field causes a change in the value of
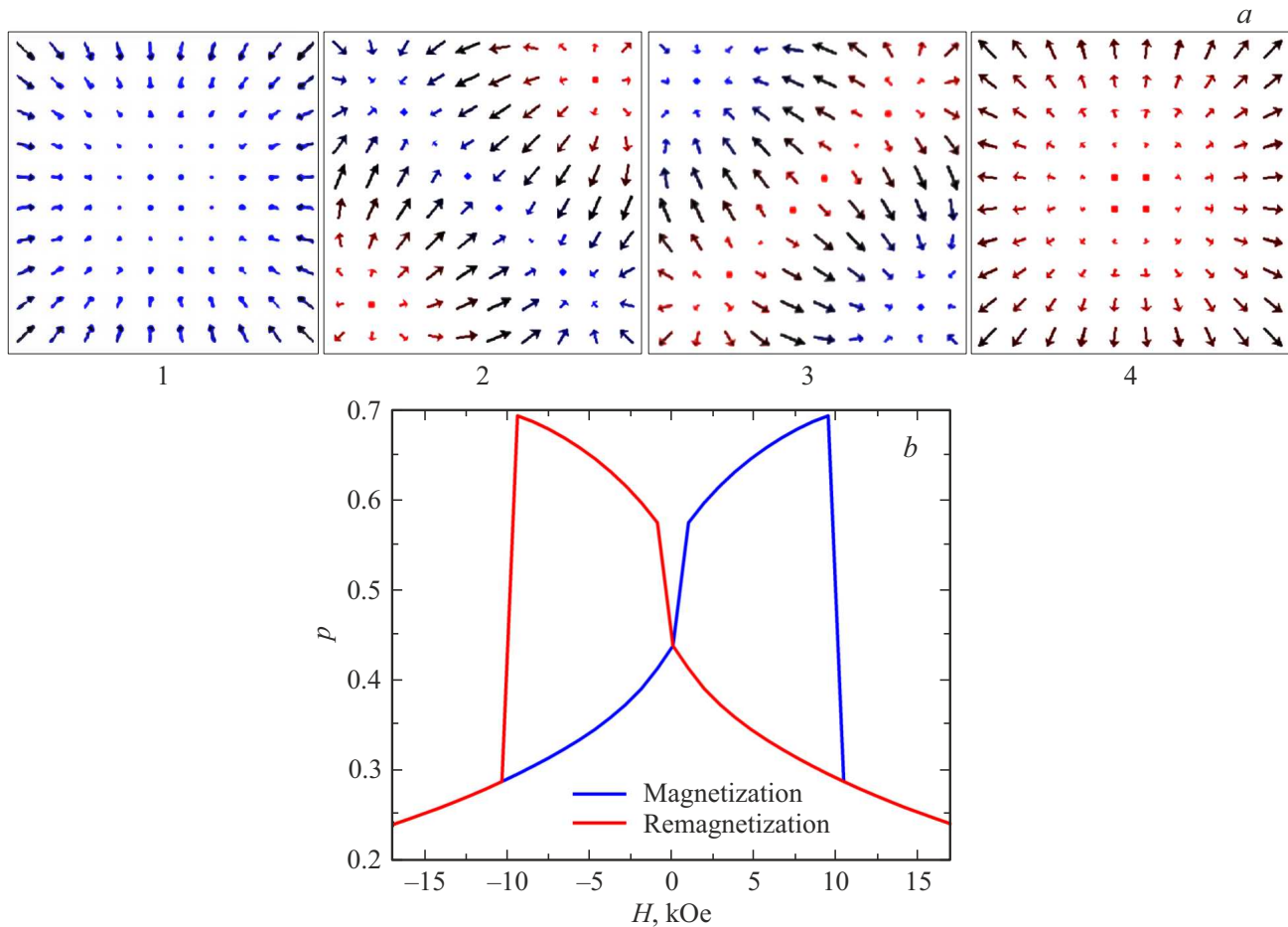
a — micromagnetic states (1, 2, 3, 4), implemented in the nano-element when changing the magnetic field; b — electric polarization dependence graph from magnetic field, $D = 0.6\,\mathrm{mJ/m^2}$, $a = 50\,\mathrm{nm}$, $t = 30\,\mathrm{nm}$.

the total electric polarization of $\mathbf{p} = \frac{1}{V} \sum_i \mathbf{P}(\mathbf{r}_i)$ (see Figure, part b).

Finally, we note several works on the study of MEE in multiferroic films. In Terfenol-D — containing composite structures [41,42], have been experimentally observed by the MEE, with hysteresis dependencies of the piezoelectric coefficients on the magnetic field being similar to the calculated polarization variation. Ref. [43] presents the results of experimental studies on the effects of DMI (Dzyaloshinskii–Moriya interactions at interface) on the magnetoelectric properties of $Sr_2IrO_4/SrTiO_3$ ($BaTiO_3$) (Ruddlesden–Popper structures on a pair/ferroelectric substrate), with the magnitude of the magnetoelectric coefficient and electric polarization in these structures regulated by DMI. Experimental study of magnetoelectric effects in the array of nano-dots in the composite structure of ferromagnetic-piezo-electric $[Pt/Co/Ta]_{12}$ taking into account DMI is performed in work [44]. The magnetoelectric effect is experimentally studied in the films of ferrite garnets [15,45], but in the absence of DMI. Nevertheless, the presented results indicate the characteristic features of polar states, which depend and are determined by the topology of magnetic inhomogeneities.

4. Conclusion

In work the magnetoelectric properties of multiferroics with the perovskite structure are investigated. The instability of the structure of ABO_3 of the perovskites to the replacement of A, B-cations results in a wide variety of magnetic structures that differ in symmetry of crystalline structure, magnetic and ferroelectric properties. The examples are multiferroics of different symmetries (trigonal — $BiFeO_3$, orthorhombic — $RCrO_3$ and $RFeO_3$, tetragonal — Ruddlesden–Popper). This allows to illustrate the influence of crystallographic distortions on the magnetic and ferroelectric properties of multiferroics. It is shown that in $RCrO_3$ and $RFeO_3$ the ferroelectric polarization ($P_s \sim 0.04\,\mu\mathrm{C/cm^2}$) can arise due to the destruction of the anti-ferroelectric structure of dipole moments formed in the neighborhood of Cr and Fe ions, unlike $BiFeO_3$, in which the spontaneous electric polarization ($P_s \sim 50-100\,\mu\mathrm{C/cm^2}$) allowed by symmetry is realized. The components of the tensors of the linear magnetoelectric effect of the considered multiferroics are calculated, the possibility of implementing a linear magnetoelectric effect in Ruddlesden–Popper structures is shown. The article

considers manifestations of inhomogeneous magnetoelectric effect in multiferroics structures of restricted geometry, shows the possibility of occurrence of polar states of different type at magnetization of such structures. Hysteresis dependencies of electric polarization and magnetization have been plotted, allowing to detect the switching of states in devices based on magnetoelectric nano-elements.

Funding

Conflict of interest

The authors declare that they have no conflict of interest.

References

[1] S. Manipatruni, D.E. Nikonov, C.-C. Lin, T.A. Gosavi, H. Liu, B. Prasad, Y.-L. Huang, E. Bonturim, R. Ramesh, I.A. Young. Nature **565**, 35 (2019).

[2] J.F. Scott, J. Floyd. npj Computat. Mater. **1**, *1*, 1–9 (2015).

[3] B. Sun, G. Zhou, L. Sun, H.B. Zhao, Y. Chen, F. Yang, Y. Zhao, Q.L. Song. Nanoscale Horizons **6**, 939 (2021).

[4] A.A. Bukharaev, A.K. Zvezdin, A.P. Pyatakov, Yu.K. Fetisov. UFN **188**, *12*, 1288 (2018) (in Russian).

[5] C.N.R. Rao, A. Sundaresan, R. Saha. J. Phys. Chem. Lett. **3**, 2237 (2012).

[6] A.M. Shikin, D.A. Estyunin, N.L. Zaitsev, D. Glazkova, I.I. Klimovskikh, S.O. Filnov, A.G. Rybkin, E.F. Schwier, S. Kumar, A. Kimura, N. Mamedov, Z. Aliev, M.B. Babanly, K. Kokh, O.E. Tereshchenko, M.M. Otrokov, E.V. Chulkov, K.A. Zvezdin, A.K. Zvezdin. Phys. Rev. B **104**, 115168 (2021).

[7] A.B. Harris. Phys. Rev. B **84**, 064116 (2011).

[8] P. Sahlot, A. Jana, A.M. Awasthi. AIP Conf. Proc. **1942**, 130009 (2018).

[9] M.V. Lobanov, M. Greenblatt, E.ad N. Caspi, J.D. Jorgensen, D.V. Sheptyakov, B.H. Toby, C.E. Botez, P.W. Stephens. J. Phys.: Condens. Matter **16**, 5339 (2004).

[10] B.H. Zhang, Z.Z. Hu, B.H. Chen, X.Q. Liu, X.M. Chen. J. Appl. Phys. **128**, 054102 (2020).

[11] G.A. Smolensky, V.A. Isupov, A.I. Agranovskaya, N.N. Kraynik. FTT **2**, 2982 (1960) (in Russian).

[12] G.A. Smolensky, I.E. Chupis. UFN **137**, *7*, 415 (1982) (in Russian).

[13] Z. Gabbasova, M. Kuz'min, A. Zvezdin, I. Dubenko, V. Murashov, D. Rakov, I. Krynetsky. Phys. Lett. A **158**, 491 (1991).

[14] J. Li, J. Wang, M. Wuttig, R. Ramesh, N. Wang, B. Ruette, A.P. Pyatakov, A.K. Zvezdin, D. Viehland. Appl. Phys. Lett. **84**, *25*, 5261 (2004).

[15] A.P. Pyatakov, A.K. Zvezdin. UFN **182**, *6*, 593 (2012) (in Russian).

[16] N.Ye. Kulagin, A.F. Popkov, A.K. Zvezdin. FTT **53**, *5*, 912 (2011) (in Russian).

[17] Z. Gareeva, O. Diéguez, J. Iñiguez, A.K. Zvezdin. Phys. Rev. B **91**, 060404 (2015).

[18] A.F. Popkov, M.D. Davydova, K.A. Zvezdin, S.V. Solov'yov, A.K. Zvezdin. Phys. Rev. B **93**, 094435 (2016).

[19] M. Lorenz, G. Wagner, V. Lazenka, P. Schwinkendorf, H. Modarresi, M.J. Van Bael, A. Vantomme, K. Temst, O. Oeckler, M. Grundmann. Appl. Phys. Lett. **106**, 012905 (2015).

[20] D. Sando, A. Agbelele, D. Rahmedov, J. Liu, P. Rovillain, C. Toulouse, I.C. Infante, A.P. Pyatakov, S. Fusil, E. Jacquet, C. Carrétéro, C. Deranlot, S. Lisenkov, D. Wang, J.-M. Le Breton, M. Cazayous, A. Sacuto, J. Juraszek, A.K. Zvezdin, L. Bellaiche, B. Dkhil, A. Barthélémy, M. Bibes. Nature Mater. **12**, *7*, 641 (2013).

[21] V.A. Murashov, D.N. Rakov, I.S. Dubenko, A.K. Zvezdin, V.M. Ionov. Kristallografiya **35**, *4*, 912 (1990) (in Russian).

[22] A. Kadomtseva, Yu.F. Popov, T.V. Schogoleva, G.P. Vorob'ev, A.K. Zvezdin, V.A. Murashov, D.N. Rakov. Ferroelectrics **169**, 85 (1995).

[23] G.P. Vorobyev, A.K. Zvezdin, A.M. Kadomtseva, Yu.F. Popov, V.A. Murashov, D.N. Rakov. FTT **37**, *11*, 3262 (1995) (in Russian).

[24] G.P. Vorobyev, A.K. Zvezdin, A.M. Kadomtseva, Yu.F. Popov, V.A. Murashov, Yu.P. Chernenkov. FTT **37**, *8*, 2428 (1995) (in Russian).

[25] V.A. Murashov, D.N. Rakov, N.A. Ekonomov, A.K. Zvezdin, I.S. Dubenko. FTT **32**, 2156 (1990) (in Russian).

[26] V.S. Pokatilov, A.S. Sigov, A.O. Konovalova, A. Gippius, N. Gerwitz. Fundamentalniye problemy radioelektronnogo priborostroyeniya **10**, *1−3*, 366 (2010) (in Russian).

[27] V.S. Rusakov, V.S. Pokatilov, A.S. Sigov, A.A. Belik, M.E. Matsnev. FTT **61**, *6*, 1107 (2019) (in Russian).

[28] J. Chen, L. Liu, X.L. Zhu, Z.V. Gareeva, A.K. Zvezdin, X.M. Chen. Appl. Phys. Lett. **119**, 112901 (2021).

[29] A.K. Zvezdin, A.A. Mukhin. Pis'ma v ZhETF **88**, *8*, 581 (2008) (in Russian).

[30] Y. Tokunaga, S. Iguchi, T.H. Arima, Y. Tokura. Phys. Rev. Lett. **101**, *9*, 097205 (2008).

[31] Z. Gareeva, A. Zvezdin, K. Zvezdin, X. Chen. Materials **15**, *2*, 574 (2022).

[33] K.P. Belov, A.K. Zvezdin, A.M. Kadomtseva, R.Z. Levitin. Orientatsionniye perekhody v redkozemelnykh magnetikakh. Nauka, M. (1979) (in Russian).

[34] E.A. Turov, A.V. Kolchanov, V.V. Menshenin, I.F. Mirsaev, V.V. Nikolaev. Simmetriya i fizicheskiye svoystva antiferromagnetikov. Fizmatlit, M. (2001). 559 s. (in Russian).

[35] B. Rajeswaran, D.I. Khomskii, A.K. Zvezdin, C.N.R. Rao, A. Sundaresan. Phys. Rev. B **86**, 214409 (2012).

[36] V.A. Sanina, B.H. Khannanov, E.I. Golovenchitz, M.P. Shcheglov. FTT **61**, *3*, 501 (2019) (in Russian).

[37] V.A. Sanina, B.H. Khannanov, E.I. Golovenchitz, M.P. Shcheglov. FTT **61**, *1*, 95 (2019) (in Russian).

[38] A.K. Zvezdin, Z.V. Gareeva, X.M. Chen. J. Phys. Condens. Matter **33**, 385801 (2021).

[39] M.J. Pitcher, P. Mandal, M.S. Dyer, J. Alaria, P. Borisov, H. Niu, J.B. Claridge, M.J. Rosseinsky. Science **347**, *6220*, 420 (2015).

[40] M.J. Donahue, D.G. Porter. OOMMF User's Guide, Version 1.0; NIST IR 6376. National Institute of Standards and Technology: Gaithersburg, MD, 1999; p NIST IR 6376.

[41] T.Z. Wang, Y.H. Zhou. J. Appl. Phys. **108**, 123905 (2010).

[42] J. Zhang, Y. Gao. Int. J. Solids Struct. **69−70**, 291 (2015).

[43] X. Liu, W. Song, M. Wu, Y. Yang, Y. Yang, P. Lu, Y. Tian, Y. Sun, J. Lu, J. Wang, D. Yan, Y. Shi, N.X. Sun, Y. Sun, P. Gao, K. Shen, G. Chai, S. Kou, C.-W. Nan, J. Zhang. Nature Commun. **12**, *1*, 5453 (2021).

[44] Z. Hou, Y. Wang, X. Lan, S. Li, X. Wan, F. Meng, Y. Hu, Z. Fan, C. Feng, M. Qin, M. Zeng, Xi. Zhang, X. Liu, X. Fu, G. Yu, G. Zhou, Y. Zhou, W. Zhao, X. Gao, J.-M. Liu. Adv. Mater. **34**, *11*, 2270090 (2022).

[45] K.S. Antipin, T.T. Gareev, N.V. Myasnikov, E.P. Nikolaeva, A.P. Pyatakov. J. Appl. Phys. **129**, *2*, 024103 (2021).